Generation of intrinsic vibrational gap modes in three-dimensional ionic crystals

S. A. Kiselev* and A. J. Sievers
Laboratory of Atomic and Solid State Physics and the Materials Science Center, Cornell University, Ithaca, New York 14853-2501
(Received 14 August 1996)

The existence of anharmonic localization of lattice vibrations in a perfect three-dimensional diatomic ionic crystal is established for the rigid-ion model by molecular dynamics simulations. For a realistic set of NaI potential parameters, an intrinsic localized gap mode vibrating in the [111] direction is observed for fcc and zinc-blende lattices. An axial elastic distortion is an integral feature of this mode which forms more readily for the zinc blende than for the fcc structure. Molecular dynamics simulations verify that in each structure this localized mode may be stable for at least 200 cycles. [S0163-1829(97)03610-2]

It has been proposed[1,2] and numerically demonstrated[3] that a large amplitude vibration in a perfect one-dimensional (1D) lattice can localize because of anharmonicity. More detailed analytical and numerical investigations of classical 1D anharmonic chains made possible by simple eigenvalue generating recursion relations have revealed a variety of stable intrinsic localized modes with frequencies outside of the plane wave bands.[3–8] Recently quantum mechanical aspects of intrinsic localized modes (ILM's) have been considered.[9,10] Some progress also has been reported for higher-dimensional classical crystal lattices with simple nearest-neighbor model interactions.[11,12] Particularly important has been the recognition that diatomic crystal potentials like the Born-Mayer-Coulomb in 1D produces an intrinsic gap mode (IGM) *between* the optic and acoustic branches instead of an ILM above the plane wave spectrum.[13] The possibility of IGM's in 3D anharmonic lattices with realistic potentials has remained elusive. One approach has been to focus on crystal surfaces and edges where harmonic localization already plays an important role.[14–16]

In this paper we demonstrate with molecular dynamics simulations that, for sufficiently large vibrational amplitude, anharmonicity can stabilize an IGM in a 3D uniform diatomic crystal with rigid ion NaI potential arranged in either the fcc or zinc-blende structure. By developing a self-consistent numerical technique for finding an intrinsic localized mode eigenvector, we have been able to show that for a given gap mode amplitude with the same potential that the localization is much stronger for a T_d symmetry site when compared to an O_h one.

To construct the stationary localized mode eigenvector for the nonlinear 3D diatomic lattice with long-range interactions, we build on techniques which have been used successfully to identify 1D anharmonic modes,[3] one of which is the rotating wave approximation. A Fourier extension of that idea for vibration in a stationary periodic mode with fundamental frequency ω, which includes the static and second harmonic for the ith particle displacement $\mathbf{r}_i(t)$, is

$$\mathbf{r}_i(t)=\sum_{n=0}^{2}\mathbf{r}_i^{(n)}\cos(n\omega t), \tag{1}$$

where $\mathbf{r}_i^{(0)}$is the distorted equilibrium position of the ith particle, and the $\mathbf{r}_i^{(n)}$'s are the time-independent amplitudes of the different harmonics. The force acting on the ith particle can also be represented by a similar Fourier series. Substituting the coordinate and force Fourier series into the classical equations of motion and equating the terms with different harmonics gives a time-independent system of nonlinear equations

$$\mathbf{F}_i^{(n)}+n^2\omega^2 m_i\mathbf{r}_i^{(n)}=0, \quad n=0,1,2. \tag{2}$$

The Fourier coefficients $\mathbf{F}_i^{(n)}$ are determined in the usual way.[13]

The procedure for finding the anharmonic localized mode eigenvector relies on first generating a fictitious dynamics for the Fourier amplitudes and then applying a version of dynamical simulated annealing.[17] The coefficients $\tilde{\mathbf{r}}_i^{(0)}$, $\tilde{\mathbf{r}}_i^{(2)}$, and $\tilde{\mathbf{r}}_i^{(1)}$ are now taken to vary with time and obey the following fictitious equations of motion:

$$\tilde{\mathbf{F}}_i^{(n)}=\mathbf{F}_i^{(n)}+n^2\omega^2 m_i\tilde{\mathbf{r}}_i^{(n)}=m_i\frac{d^2\tilde{\mathbf{r}}_i^{(n)}}{dt^2}, \quad n=0,1,2; \tag{3}$$

so that dynamical simulated annealing can be used to find the equilibrium values for these quantities $\mathbf{r}_i^{(0)}$, $\mathbf{r}_i^{(2)}$, and $\mathbf{r}_i^{(1)}$, when all $\tilde{\mathbf{F}}_i^{(n)}(\mathbf{r}_i^{(n)})=0$. Our iterative procedure to obtain the eigenvector is as follows.

(i) Guess an initial shape for the gap mode eigenvector. In our case we use the mass-defect eigenvector associated with a harmonic gap mode of frequency ω. The rescaled mass-defect gap mode eigenvector gives initial amplitudes $\tilde{\mathbf{r}}_i^{(1)}$ where $\mathbf{r}_0^{(1)}=\alpha$ while $\tilde{\mathbf{r}}_i^{(0)}$, $\tilde{\mathbf{r}}_i^{(2)}$, and the initial velocities are set to zero.

(ii) Make a molecular dynamics (MD) time step by solving Eqs. (3) and update the quantities, $\tilde{\mathbf{r}}_i^{(n)}$and the $\tilde{\dot{\mathbf{r}}}_i^{(n)}$ for fixed central particle amplitude α. The classical equations of motion are integrated using the ''leap-frog'' algorithm[18] with a time step of 1.35 fs.

(iii) Apply a form of dynamical simulated annealing.[17] During a MD simulation run, the oscillatory values of the kinetic energies of each of these three objects $\tilde{\mathbf{r}}_i^{(n)}$per particle for the N particles is monitored. (Each object vibrates around its equilibrium position $\mathbf{r}_i^{(n)}$.) When the total kinetic energy of the system of objects passes through its maximal value in the MD fictitious time evolution, all objects' velocities $\tilde{\dot{\mathbf{r}}}_i^{(n)}$

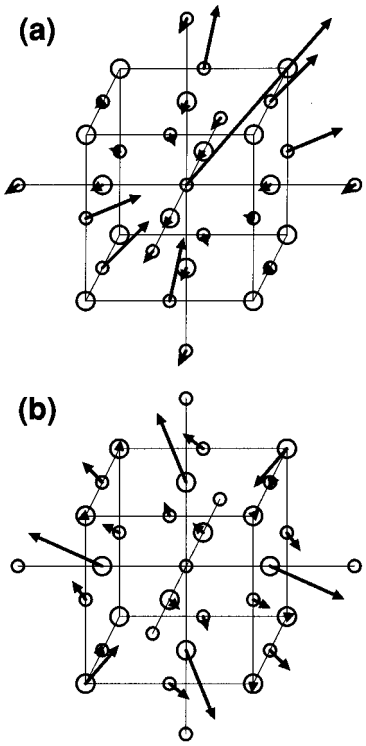

FIG. 1. The intrinsic gap mode eigenvector in the NaI crystal with fcc structure. The mode has a relative amplitude $\alpha/d=0.244$ and a relative frequency $\omega/\omega_+=0.950$. Panel (a) shows the first harmonic part of the eigenvector. The arrows represent 10× actual amplitudes for clarity. Panel (b) shows the dc part of the eigenvector. The arrows representing the displacements are expanded 40× for clarity. Small circles, Na^+ ions; large circles, I^- ions. Although not clear from the figure the magnitudes of the dc distortion for the nearest I^- ion shell are the same, consistent with an axial distortion around the [111] axis.

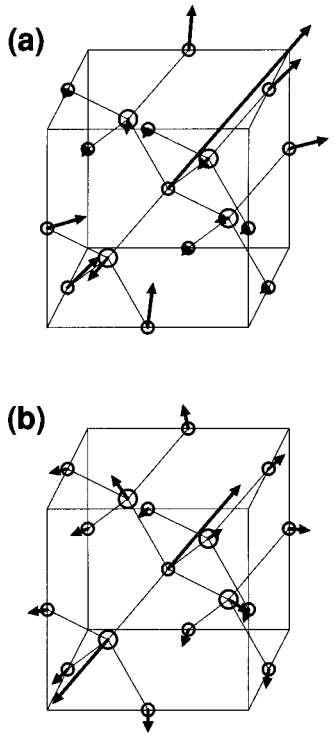

FIG. 2. The intrinsic gap mode eigenvector for a hypothetical NaI crystal with zinc-blende structure. The mode has a relative amplitude $\alpha/d=0.116$ and a relative frequency $\omega/\omega_+=0.950$. Panel (a) shows the first harmonic part of the eigenvector. The arrows represent 20× actual amplitudes. Panel (b) shows the dc part of the eigenvector. The arrows representing the displacements are expanded 40×. Small circles, Na^+ ions; large circles, I^- ions.

are set to zero. In this way we incrementally move the system closer to its equilibrium configuration.

(iv) After 40 MD steps as described in (ii) and checking for condition (iii) the intrinsic gap mode frequency ω is updated by solving the single Eq. $\mathbf{F}_0^{(1)}+\omega^2 m_0 \mathbf{r}_0^{(1)}=0$ for ω with $\mathbf{r}_0^{(1)}=\alpha$.

(v) Verify the correctness and stability of the resultant IGM eigenvector with a regular MD simulation. Repeat (i) through (iv) until the lifetime of the mode remains unchanged when the resultant eigenvector is used as an initial condition for a MD simulation. As long as the frequency of the mode remains in the gap we find the procedure described here converges to a *localized* eigenvector. No change in the results is observed when this procedure is repeated with a $\frac{1}{2}$ time step.

To investigate the possibility of a 3D intrinsic gap mode in ionic crystals we use the tabulated rigid ion potential for NaI from Tables II and IV of Ref. 19. The potential has the following form:

$$\phi(r_{ij})=\frac{z_i z_j e^2}{4\pi\epsilon_0 r_{ij}}+\frac{b}{r_{ij}^4}\exp[-k(r_{ij}-r_{0ij})]-\frac{c_{ij}}{r_{ij}^6}-\frac{d_{ij}}{r_{ij}^8}, \tag{4}$$

with r_{ij} the distance between the ions i and j, z_i and z_j are the ± 1 charges, ϵ_0 is the permittivity of vacuum, r_{0ij} is the sum of the ionic radii, b and k are parameters determined by fitting the thermal expansion and isothermal compressibility, c_{ij} and d_{ij} are respectively the coefficients for the dipole-dipole and dipole-quadrupole interactions. The lattice constant for the fcc structure is chosen to be $a=6.35$ Å, within 1% of the experimental value.[20] The calculated TO frequency is $\omega_{\mathrm{TO}}=2.51\times10^{13}$ rad/s, within 5% of the experimental value of 2.39×10^{13} rad/s.[20] The gap between the optic and acoustic branches extends from $\omega_+=2.41\times10^{13}$ rad/s to $\omega_-=1.46\times10^{13}$ rad/s.

In carrying out the MD calculations on a 216-ion cube with periodic boundary conditions the method of Sangster and Dixon[21] has been used to evaluate the Ewald sum. For this method the cutoff distance in real space is approximately half the length, $L/2$, of the cube (the interaction of the sixth neighboring shell is counted), and the reciprocal lattice is summed with the convergence parameter of $5.6/L$.

The resulting intrinsic gap mode eigenvector for the fcc NaI crystal is shown in Fig. 1. Panel (a) identifies the first harmonic part of the vibrational eigenvector $\mathbf{r}_i^{(1)}$, localized on a central light Na^+ ion and its neighboring shells with the central Na^+ ion vibrating in the [111] direction. The vibrational amplitude of the central Na^+ ion to the nearest-neighbor (NN) distance, d, $r_0^{(1)}/d=\alpha/d=0.244$. The gap mode frequency lies 5.0% below the bottom of the optic

TABLE I. Maximum amplitude in a shell versus shell index for Figs. 1 and 2. Both the vibrational amplitude and the dc distortion are given as fractions of the NN distance.

	fcc		Zinc blende	
Shell	Vib. amp.	dc dist.	Vib. amp.	dc dist.
0	0.2438	0	0.1156	0.0291
1	0.0119	0.0244	0.0147	0.0220
2	0.0734	0.0074	0.0242	0.0064
3	0.0025	0.0132	0.0005	0.0039
4	0.0149	0.0078	0.0039	0.0038

band. The elastic distortion is characterized by the dc part of the mode's eigenvector $\mathbf{r}_i^{(0)}$, which is shown in panel (b) of Fig. 1.

The above procedure has also been performed on a larger array of particles to insure that the periodic boundary conditions do not influence the results. In a 1000 ion crystal the IGM with amplitude $\alpha/d=0.244$ has the same eigenvector as shown in Fig. 1 and its frequency differs by 1% from that for the 216 ions NaI crystal. This frequency difference is associated with a slightly different crystal distortion between the two cases. The MD simulation test shows that the IGM remains stable in the large crystal and its lifetime increases slightly.

In order to investigate the role of point group symmetry on the intrinsic gap mode parameters the zinc-blende structure has also been tested with the same potential. (A local minimum of the lattice energy occurs at the slightly larger lattice constant, $a=7.00$ Å.) The IGM eigenvector for 216 particles is shown in Fig. 2. Again the central ion vibrates in the [111] direction. This mode has an amplitude to NN distance, $r_0^{(1)}/d=\alpha/d=0.116$. Again the mode vibrational eigenvector $\mathbf{r}_i^{(1)}$, is localized on a central light Na^+ ion and its neighboring shells. Note that although the relative mode amplitude is only one half that of the IGM shown in Fig. 1, its relative frequency occurs at the same value in the gap (5.0%) due to the larger elastic distortion in the zinc-blende lattice near the mode center. The maximum vibrational amplitude and dc distortion for each of the shells of particles shown in Figs. 1 and 2 are given in Table I.

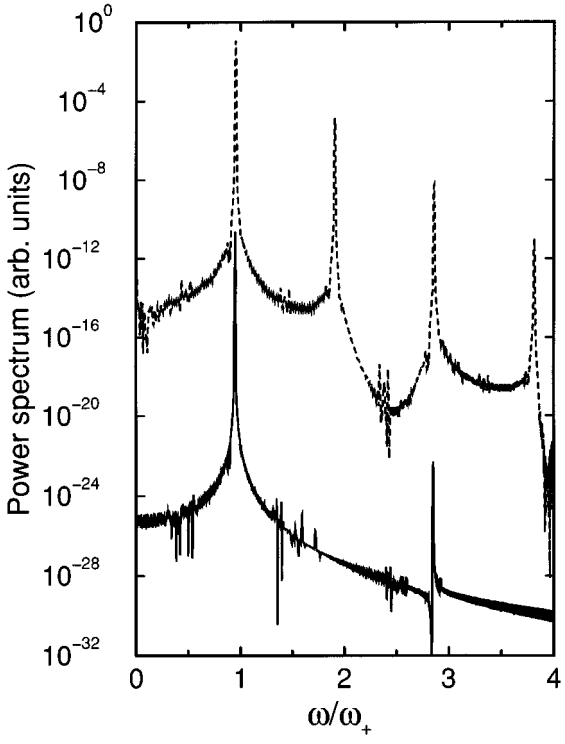

FIG. 3. The power spectrum of the central particle vibration for an IGM in an NaI crystal with either fcc or zinc-blende structure. The eigenvectors shown in Figs. 1 and 2 are used as the initial conditions for the MD simulations. The solid curve (fcc lattice) is shifted down by ten decades from the dashed curve (zinc blende) for clarity. The noise is associated with truncational errors.

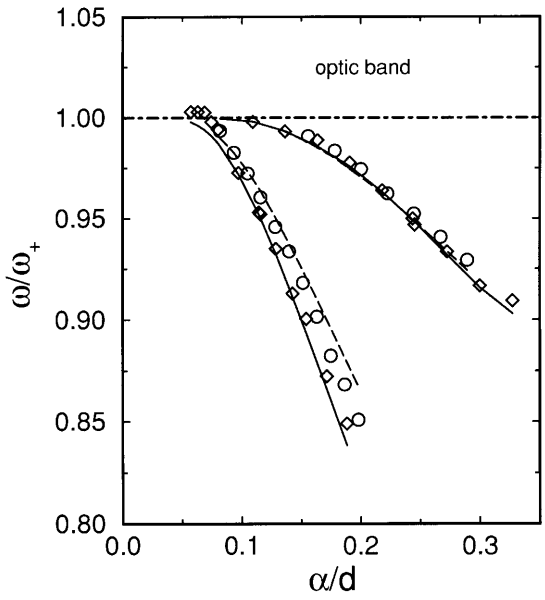

FIG. 4. The frequency of an intrinsic gap mode as a function of normalized amplitude, α/d. The left set of data are for the zinc blende and the right set for the fcc lattice. The numerical solutions of Eq. (2) are represented by the solid lines for the [111] and by dashed lines for the [110] crystal direction. The result of MD simulations are given by the open diamonds for the [111] direction and by open circles for the [110] direction.

Typical power spectra of the central particle vibration is presented in Fig. 3 for the eigenvectors shown in Figs. 1 and 2 after about 200 vibrations. These spectra reflect the stable vibration of the IGM at frequencies close to the values predicted by Eq. (2) both for the fcc and zinc-blende structures. Note that the vibrational mode for the O_h symmetry site shows a weak third harmonic while the IGM for the T_d symmetry site shows all harmonics.

Figure 4 shows the IGM frequency versus the amplitude for the two structures under investigation. The left sets of data are for zinc blende and the right sets are for the fcc lattice. These results indicate that the T_d symmetry site appears to support more anharmonicity in the sense that for a given vibrational amplitude the frequency of the IGM drops farther into the forbidden gap and has a larger elastic lattice distortion around the IGM center [compare Figs. 1(b) and 2(b)].

The general behavior of the IGM frequency versus ampli-

tude shown in Fig. 4 is similar for both structures—with increasing mode amplitude the frequency drops farther into the gap. An amplitude threshold is evident. An IGM which has its frequency about 5% below the bottom of the optics band (corresponding to the middle regions of the curves in Fig. 4) has the longest lifetime of ~200–250 vibrational periods. If its frequency drops farther into the forbidden gap (~10%) the mode's lifetime decreases to ~100 periods. At the opposite small amplitude limit its lifetime again decreases (~40 periods) presumably because of the strong coupling between the IGM and the nearby plane waves.

In both systems the elastic distortion associated with the IGM has lower symmetry than the corresponding point group symmetry of the crystal. To recover the full crystal point group symmetry for this perfect crystal it must be possible with a different set of initial conditions to rotate the IGM about the equilibrium lattice site. To test this idea we have examined IGM excitations along the three different crystal directions. Although a stable IGM mode does not appear for initial excitation along the [100] direction, the dashed lines and open circles in Fig. 4 demonstrate that for both point group symmetries a [110] directed mode can occur. These sets of data support the idea of an interchange of the IGM vibration direction as would be expected, for example, with hindered rotational motion of the excitation about the lattice site. This concomitant low-frequency component of the IGM may provide new experimental ways to excite and identify these nonlinear excitations.

We thank S. R. Bickham, G. V. Chester, R. H. Silsbee, and M. P. Teter for helpful discussions. This work is supported in part by Grant Nos. NSF-DMR-931238, ARO-DAAH04-96-1-0029, and the MRL central facilities. Some of this research was conducted using the resources of the Cornell Theory Center, which receives major funding from the National Science Foundation and New York State, with additional support from other members of the center's Corporate Partnership Program.

*Permanent address: Institute of Spectroscopy of Russian Academy of Sciences, Troitsk, Moscow 142092, Russia.

[1] A. S. Dolgov, Sov. Phys. Solid State **28**, 907 (1986).
[2] A. J. Sievers and S. Takeno, Phys. Rev. Lett. **61**, 970 (1988).
[3] V. M. Burlakov, S. A. Kiselev, and V. N. Pyrkov, Phys. Rev. B **42**, 4921 (1990).
[4] J. B. Page, Phys. Rev. B **41**, 7835 (1990).
[5] K. W. Sandusky, J. P. Page, and K. E. Schmidt, Phys. Rev. B **46**, 6161 (1992).
[6] Y. S. Kivshar and N. Flytzanis, Phys. Rev. A **46**, 7972 (1992).
[7] S. A. Kiselev, S. R. Bickham, and A. J. Sievers, Comments Condens. Matter Phys. **17**, 135 (1995).
[8] A. Franchini, V. Bortolani, and R. F. Wallis, Phys. Rev. B **53**, 5420 (1996).
[9] T. Rössler and J. B. Page, Phys. Rev. B **51**, 11 382 (1995).
[10] W. Z. Wang, J. Tinka Gammel, A. R. Bishop, and M. I. Salkola, Phys. Rev. Lett. **76**, 3598 (1996).
[11] S. Takeno, J. Phys. Soc. Jpn. **58**, 3899 (1990).
[12] S. Flach, K. Kladko, and C. R. Willis, Phys. Rev. E **50**, 2293 (1994).
[13] S. A. Kiselev, S. R. Bickham, and A. J. Sievers, Phys. Rev. B **48**, 13 508 (1993).
[14] J. N. Teixeira and A. A. Maradudin, Phys. Lett. A **205**, 349 (1995).
[15] D. Bonart, A. P. Mayer, and U. Schröder, Phys. Rev. Lett. **75**, 870 (1995).
[16] D. Bonart, A. P. Mayer, and U. Schröder, Phys. Rev. B **51**, 13 739 (1995).
[17] R. Car and M. Parrinello, Phys. Rev. Lett. **55**, 2471 (1985).
[18] R. W. Hockney and J. W. Eastwood, *Computer Simulation Using Particles* (McGraw-Hill, New York, 1981).
[19] J. Michielsen, P. Woerlee, F. V. D. Graaf, and J. A. A. Ketelaar, J. Chem. Soc. Faraday Trans. II **71**, 1730 (1975).
[20] M. J. L. Sangster, U. Schröder, and R. M. Atwood, J. Phys. C **11**, 1523 (1978).
[21] M. J. L. Sangster and M. Dixon, Adv. Phys. **25**, 247 (1976).